Global NEST Journal, Vol 26, No 2, 05180

Transport of alumina nanoparticles in natural waters and water saturated porous media-an analysis of the effect of various environmental parameters

Pavan kumar Chilakapati and Mrudula Pulimi*
Centre for Nanobiotechnology, Vellore Institute of Technology, Vellore, Tamil Nadu, India
Received: 06/06/2023, Accepted: 04/12/2023, Available online: 12/12/2023
*to whom all correspondence should be addressed: e-mail: pmrudula@vit.ac.in
https://doi.org/10.30955/gnj.005180

Graphical abstract

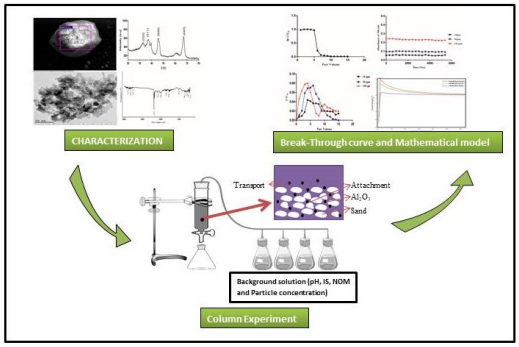

Abstract

To control the use and disposal of products containing nanoparticles and lessen the risks they pose to soil and aquatic ecosystems, it is essential to understand the fate and transport of Al_2O_3 NPs. The stability, settling, retention, and transport of Al_2O_3 NPs in aqueous environments and saturated sand media were investigated in the current work to determine how solution chemistry and water chemistry influenced these processes. There was a notable rise and variety in settling of nanoparticles in different water stream and simulated aqueous solutions under static aqueous circumstances. The impact of solution chemistry in the transport of the nanoparticles was also examined in a column filled with quartz sand and various combinations of ionic strength (10 to 100 mM of NaCl), pH (3 to 7), natural organic matter (0.1 to 10 ppm of Humic acid), and natural water systems. The results demonstrate that the environmental conditions may significantly affect the transport and retention of nanoparticles, with humic acid exhibiting enhanced movement and natural clay, Kaolinite, increasing retention. Additionally, with natural waters the transport profiles were altered. The combination of DLVO and Clean bed filtration theory provided further assistance in the prediction of the aggregation and transport of the Al_2O_3 NPs.

keywords: Aluminium oxide nanoparticle, transport, natural waters, colloid filtration theory and DLVO theory

1. Introduction

In the recent years engineered nanoparticles (ENPs), manufactured to obtain unique physicochemical features and function, were being used for a diverse application in varieties of field such as electrical, biomedical, pharmaceutical and environmental application (Davoudi *et al*. 2014; Jiang *et al*. 2009). Although there are a wide variety of engineered nanomaterials, metal oxides like titanium oxide, aluminum oxide and zinc oxide are extensively being utilized for cosmetics, engineering, water treatment and medicinal application (Bayat *et al*. 2015). Among the metal oxides, Aluminium oxide nanoparticles (Al_2O_3) is one of the utmost utilized pulverized residues in the world, the marketing percentage is growing about 5.8% to annual rate (Zheng *et al*. 2019).

Al_2O_3 Nanoparticles (Al_2O_3NPs) have unique capabilities and possess high surface area, low electrical conductivity, greater sorption potential and heat conductivity (Hassanpour *et al*. 2018; Rahman *et al*. 2013; Zheng *et al*. 2019). They has a wide range of commercial and industrial application and are also utilized in the production of fuel, in light bulbs, fluorescent tubes, flame retardant agent, and paints and also used as advanced ceramics (Hassanpour *et al*. 2018; Zheng *et al*. 2019). Further, Al_2O_3 NPs have been used for biological applications which include biosensors, biofilters, medical administration, antigen delivery for vaccination and bactericides. (Witharana *et al*. 2012).

Because of the widespread use of Al_2O_3 NPs, they will ultimately reach the subsurface and water bodies, while their transportation and fate mechanism are still unidentified and may have toxic effect on human life (Davoudi *et al*. 2014). Therefore, to access the potential risk of the Al_2O_3 NPs to human health, it is necessary to recognize their fate and transit into natural system. The nanoparticle aggregation and settling are critical in understanding the retention and transit through the soil and water ecosystems and needs additional investigation (Witharana *et al*. 2012).The colloidal behavior of Al_2O_3NPs in one of the key elements influencing its fate, transit and toxicity into the system (to both natural, human, plant and

animal system) (S. Ghosh *et al*. 2008).The nature of the manufactured colloidal nanoparticles in ecosystem is influenced by various parameters including pH, IS and the presence of NOM present in the nature.

Many studies are available in literature which inspect the deposition, transit and retention of nanoparticles in saturated porous media due to the environmental concern and the potential risk. Surface charge, size of the particles, surface and core chemistry, flowrate, ionic strength (IS), presence of organic matter, porousness of media, pH, aggregation, and other physio-chemical variables can all influence nanoparticle transport in porous media. As a result, understanding the complex interactions of the physico-chemical parameters involved in the transport and deposition of designed nanomaterials is critical. However, for Al_2O_3 NPs, the processes underlying elution and retention have not been thoroughly evaluated (Rahman *et al*. 2013). The clay minerals are also an important component of natural aquifer soil, because they frequently contain multiple of amphoteric sites under common environmental condition and as a result may have significant impact on the transport of both positively and negatively charged nanoparticle by providing favorable deposition sites. Subsurface porous medium frequently contains different types of clay minerals with varying physicochemical characteristics. As a result various clay minerals may have varying effects on particle mobility (Lu *et al*. 2021). The majority of recent studies were directed towards the Al_2O_3 NPs environmental behavior in lab-based pure water. Therefore, Al_2O_3 NPs environmental behavior in a natural water system required attention. In order to lessen the toxicity of Al_2O_3 NPs after their release into the natural system, it is necessary to investigate the impact of water chemistry and associated processes in the natural water systems (D. Kumari and Rychoudhury 2020).

The chief purpose of this paper was to measure the stability of Al_2O_3 NPs suspension under various solution chemistry pH (3, 5 and 7), IS (NaCl 10, 50 and 100mM) and Natural organic matter (Humic acid (HA) 0.1,1 and 10 ppm) and also on their retention and transport in saturated porous media. Also, the packed column comprising quartz sand mixed with clay mineral (Kaolinite) was utilized to investigate the mechanism of influence of clay mineral deposits on the movement of Al_2O_3 NPs. Further, the experimental data was supported with DLVO and CFT theory for the justification of mobility trends in batch and column studies.

2. Materials and method

2.1. Porous media

Ultrapure Quartz sand (50 -70 mesh particle size) was procured from Sigma Aldrich - Merck, and was used as a model porous media for replicating coarse sand in natural habitats and NPs transport studies in the current investigation. The Quartz sand was pretreated with hydrochloric acid for 24 hours, then rinsed extensively with DI water and annealed at 100◦ c using hot air oven. Potentiometric titration method was used to estimate the point of zero charge of the quartz sand. Under the experimental conditions, the crushed quartz sand's zeta potentials were also measured (Brookhaven Instruments Corporations, USA) (Rahman *et al*. 2013; Solovitch *et al*. 2010).

2.2. Metal oxide nanoparticles

Al_2O_3NPs (99.8% pure) with 50 nm nominal size were procured from Merck, India. Prior to use, the Al_2O_3 nano-powder was dissolved in ultrapure water and sonicated at 550W for 30 minutes with ultra-sonicator (Sonics, USA). The ionic strength (IS) of aluminum oxide (Al_2O_3) suspensions were adjusted from 10 to 100 mM using NaCl solution. The suspension pH was adjusted to 3,5, and 7 by the addition of 0.1 M HCl or 0.1 M NaOH. As a model natural organic matter (NOM)chemical, humic acid (HA) was used. The 50ppm HA stock was made by dissolving humic acid (HA) powder in milli-q water, spinning it for 24hrs with a magnetic stirrer, and filtrating it using a syringe filter. Particle size and surface charge of the NPs suspension at various concentration of HA (0.1,1and 10ppm), IS (10,50, and 100mM), and at varying pH was measured by zeta-sizer (Brookhaven Instruments Corporations, USA). All experimental procedures were executed in triplicates at ambient temperature (25°C). The Table 1 illustrates the zeta potential values and size distribution of the Al_2O_3 suspensions obtained in above mentioned suspension (Jones and Su 2014).

Table 1. Size and charge distribution of Al_2O_3

Parameters	Particle size (µm)	Zeta Potential (mV)
pH 3	0.216±0.0556	24.57
pH 5	0.408±0.0315	22.72
pH 7	0.608±0.025	25.03
10 mM (NaCl)	0.672±0.411	10.05
50 mM (NaCl)	1.166±0.008	25.21
100 mM (NaCl)	1.444±0.078	27.2
0.1 mg/L HA	1.06±0.399	-28.3
1 mg/L HA	0.61±0.088	-25.95
10 mg/L HA	0.441±0.031	-36.09
10 mg/L	0.454±0.098	-25.53
50 mg/L	0.365±0.046	-26.8
100 mg/L	0.991±0.055	-28.07
Ground water	16.45±24.388	-8.9
Lake water	8.512±4.717	-0.04
River water	2.123±0.171	-5.19
Tap water	4.191±0.727	0.34

2.3. Characterization

X-ray diffraction (XRD), Fourier Transform Infrared spectroscopy (FTIR), Transmission Electron Microscopy (TEM), zeta potential measurements and particle size were used to characterize the Al_2O_3. The XRD pattern was created using a Bruker equipment using Cu Kα radiation (λ= 1.5418Å). IRAffinity-1, Shimadzu, USA was used to capture the FTIR spectra. The adsorption spectra were obtained in the 400-4000 cm^{-1} range. SEM (ZEISS(EV018)) and TEM (FEI Tecnai G2 TWIN) was used to examine the morphology, topography and particle size distribution of Al_2O_3. Using Zeta-sizer (Brookhaven Instruments Corporation, USA), examined the zeta potentials and particle sizes of Al_2O_3NPs suspension. Energy Dispersive X-Ray Analysis (EDX)

(ZEISS(EV018)) used to regulate the elemental makeup of materials.

2.4. Characterization of natural water

The ground water was collected from one of the well located in Kathalampattu R.F., Tamil FNadu, India (12.772605º; 79.08391º). The river water was collected from Naganathi river, Puthur R.F., Tamil Nadu (12°43'47.2"N 79°03'23.1"E), Lake water was collected from VIT Lake, (12.96938804045568, 79.16025254404639), Vellore, Tamil Nadu and the Tap water was collected from the municipal water (12°58'06.4"N 79°08'48.6"E) of Vellore, Tamil Nadu. All the water were filtered before analyzing the composition. (Glens innovation Lab, Pvt. Ltd., Chennai) (Zhou and Keller 2010).

2.5. Sedimentation experiment

The rate of sedimentation was studied at various concentration of Al_2O_3 (10, 50 and 100ppm), pH (3, 5 and 7), IS (10, 50 and 100mM) and HA (0.1, 1 and 10ppm) as well as natural water samples for 90 min in glass beakers. Every 5mins interval, 1ml of the sample was collected and the NPs concentration was measured by taking the absorbance of every sample using UV-Visible spectrophotometer (Jenway 6850) (Khan *et al*. 2018; Zhang *et al*. 2008).

2.6. Column transport experiment in different solution chemistry

2.6.1. Experimental setup

The experiments were conducted using an Econo column (1.5*10 cm diameter* length) from Bio-Rad Laboratories, which was filled to a depth of 50 mm with sand. A diagram of the investigational setup for column studies is shown in Figure 1.

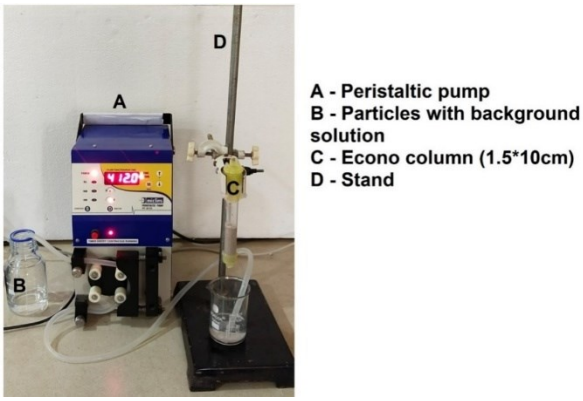

Figure 1. Experimental setup for column

2.6.2. Bromide tracer test

The hydraulic parameters of the column were measured by performing a bromide tracer test with bromide salt of potassium as a tracer chemical. To make bromide suspension, 1mg/L of KBr was mixed in 1mM NaCl solution. The bromide conc. from the tracer test was restrained using bromide ion sensor. The distribution volume of the column was measured using the convection diffusion equation (ADE).

The porousness of the sand was determined by the square summation of investigational result and the ADE solution for each sample collected from the outlet using the least-square approach. With a correlation value of 0.998, tracer tests reveal the data is perfect fit (Figure 2). The tracer tests were performed at different time intervals and the mean porousness was determined to be 0.408 ± 0.012 (Rahman *et al*. 2014).

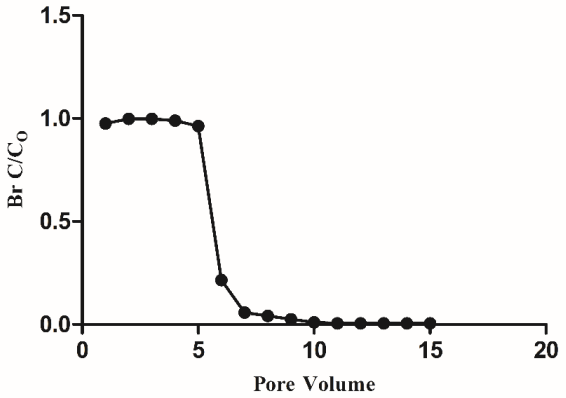

Figure 2. Bromide tracer experiment fit using Advection Dispersion Equation. C_0 and C represent the conc. of bromide in inlet and outlet, respectively

2.6.3. Transport experiment

After filling the column with Quartz sand, the columns were pre-equilibrated with 10 pore volumes of the background suspension at constant IS and pH. Four pore volumes of NPs suspension were added to the column following pre-equilibration, followed by ten pore volumes of NaCl solution having similar experimental parameters of background suspension, and five pore volumes of ultra-pure water. A peristaltic pump has been used to inject the solutions into the columns in a downward flow (Mic—Lins pp-30EX). At the time of column experiments, NPs suspension are sonicated on a regular basis to avoid NPs settlement and maintain suspension stability at the preferred suspension chemistries. The transport studies were accomplished at three ionic strengths (10, 50, and 100 mM) in NaCl, pH conditions (pH 5, 7, and 9) and HA (0.1, 1 and 10ppm). The Concentration of the nanoparticles in collected samples were measured by using UV-Spec (Jenway 6850) at 360nm. (J. Kumari *et al*. 2016). To investigate the influence of suspended clay particle, kaolinite was utilized as model clay. For transport studies, the kaolinite powder was mixed with quartz sand in the range of 0.1, 0.5 and 1% and then they were loaded slowly into the column. To study the environmental behavior of Al_2O_3, the transportation experiment was carried out with river, lake, ground and tap water collected from various sources mentioned in the above section. In order to replicate the flow conditions in aquifer sediments, the flow rate of all experiments was set to (1mL/min) (Lu *et al*. 2021).

2.7. Mathematical model

2.7.1. DLVO Interaction energy

The potential interaction energies between Al2O3 NPs with each other and with collector surface were estimated based on the classical Derjaguin–Landau–Verwey–Overbeek (DLVO) theory (Derjaguin 1941; Verwey et al. 1948). According to the theory, the total interaction energy between the colloidal particles and the collector surface is the sum of van der waals attraction forces and the electrostatic double layer repulsion forces. In this study, the van der waals interaction energy was estimated based on the assumption that the surface potential is constant for sphere – sphere and sphere – plane interaction (Gregory 1981; Sun *et al*. 2015). The electrostatic interaction energy profiles were derived based on the method proposed by Hogg *et al*. 1966 and Kang *et al*. 2015.

2.8. Clean bed filtration model

The clean bed filtration model is the most commonly used model for elucidating the path of a colloidal particle through a porous media. Gravitational deposition, Interception and diffusion are the processes involved in the association of the suspended particles with the surface of the porous media. Assuming laminar flow conditions and negligible particle-particle interactions, the extent on of advection, dispersion and deposition of the nanoparticles is represented by the 1D advection-dispersion equation (ADE) (Equation 1). The deposition rate is considered to be first order and depends on the aqueous phase concentration of the nanoparticles described by equation 2.

$$\frac{\partial C}{\partial t}+\frac{\rho b}{\theta w}\frac{\delta S}{\delta t}=D\frac{\partial^2 C}{\partial X^2}-\vartheta\frac{\partial C}{\partial X} \quad (1)$$

$$\frac{\rho b}{\theta w}\frac{\partial S}{\partial t}=k_{att}C \quad (2)$$

Where, C and S are the concentrations of the nanoparticles in the liquid and solid phase respectively, v is particle velocity, D is Coefficient of Hydrodynamic dispersion, θw is porosity of the column, ρb - Bulk density of porous medium and k_{att} is particle deposition rate coefficient. The experimentally determined coefficient of particle deposition rate is related to single collector efficiency (η_0) and the attachment efficiency (α) by

$$k_{att}=\frac{3\,(1-\theta_w)v}{2d_c}\eta o^{\alpha} \quad (3)$$

Where η_0 is estimated by using the equation proposed by Tufenkji and Elimelech,2004(Tufenkji and Elimelech 2004), and α by using the column retention profiles based on the below equation:

$$\alpha_{BTC}=-\frac{2d_c}{3(1-\varepsilon)\eta_o L}In(C_L-C_o) \quad (4)$$

Where d_c – the average size of collector particles, ε – porosity, L – column height, and C_0 and C_L – particle concentrations in the inlet and outlet, respectively. (Jones and Su,2014) MATLAB,2020 was used to perform all the relevant calculations.

3. Results and discussion

3.1. Characterization

The chemical structures and morphology of Al_2O_3NPs were studied XRD, FTIR, EDX, SEM and TEM. Figure 3a shows an XRD pattern of a distinct single crystal phase corresponding to the cubic lattice of Al_2O_3. The Al_2O_3 showed peaks at 2θ values of 32.60°, 38.49°, 46.71°, 67.94° which correspond to reflection (220), (311), (400), (440) planes. By matching the peaks to the JCPDS number 00-029-0063, the peaks were verified. The crystal size was measured by Debye Scherer's method. The average crystal size of Al_2O_3 was around 12 nm (Alamouti *et al*. 2021; Nila 2018; Prashanth*et al*. 2015).

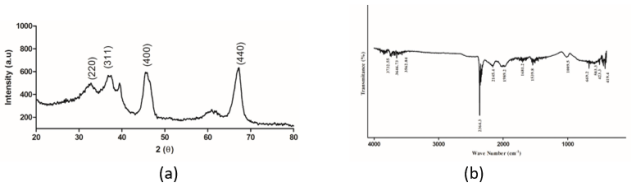

(a) (b)

Figure 3. XRD (a) and FTIR (b) pattern of Al_2O_3

The FTIR pattern of Al_2O_3 NPs was shown in Figure 3b, and the FTIR peak assignments were clearly listed in Table 2. (Alamouti *et al*. 2021; Nila 2018; Prashanth *et al*. 2015).

Table 2. FTIR spectrum assignments for Al_2O_3 NPs

Wave Number (cm^{-1})	Vibration Type	Assignment	Reference
669.2 and 503.3 cm^{-1}	Stretching	Al-O-Al	(Alamouti *et al*. 2021; Nila 2018; Prashanth *et al*. 2015)
1009.5 cm^{-1} and 2364.3 cm^{-1}	Stretching	C-O	(Alamouti *et al*. 2021; Nila 2018; Prashanth *et al*. 2015)
3732.5 cm-1, 3636.7 cm^{-1}	Stretching	O-H (aluminum hydroxide)	(Alamouti *et al*. 2021; Nila 2018; Prashanth *et al*. 2015)
3562.8 cm^{-1}, 2145.4 cm-1, 1681.2 cm^{-1}, and 1539.8 cm^{-1}	Stretching	O-H	(Alamouti *et al*. 2021; Nila 2018; Prashanth *et al*. 2015)
423.3 cm^{-1} and 419.4 cm^{-1}	-	AlO_4 bonds	(Alamouti *et al*. 2021; Nila 2018; Prashanth *et al*. 2015)

The SEM picture (Figure 4a) of Al_2O_3 was made up of porous and homogeneous aggregates of varying sizes. The EDX analysis (Figure 4b) shows the purity of the sample as only aluminum and oxygen were identified. The average atom percent of O and Al is 63.63 and 36.37%, respectively (Prashanth *et al*. 2015).

The TEM image (Figure 4c) demonstrates the Al_2O_3NPs are in nano regime (average particle size of 10 to 20 nm) highly

crystalline (polycrystalline) in nature (Prashanth *et al*. 2015).

3.2. Characterization of natural water

The components present in the collected natural water was clearly characterized and mentioned in the Table 3.

Table 3. Components of collected natural water samples

Content	Turbidity (NTU)	Chloride (Cl) mg/L	Sulphate (SO_4) mg/L	Hardness ($CaCO_3$) mg/L	Heavy Metals (cadmium, Lead, mercury and nickel) mg/L	TOC mg/L	Chemical oxygen demand mg/L	Dissolved Oxygen mg/L	Biochemical oxygen demand mg/L
Tap water	> 0.1	590	73	983	BLQ(LOQ:0.002)	BDL (DL:2)	BDL (DL:4)	5.5	BDL (DL:2)
Lake water	> 0.1	900	71	894	BLQ(LOQ:0.002)	BDL (DL:2)	BDL (DL:4)	5.1	BDL (DL:2)
Ground water	> 0.1	100	60	447	BLQ(LOQ:0.002)	BDL (DL:2)	BDL (DL:4)	5.3	BDL (DL:2)
River water	1.5	30	28	177	Nickel 1.02 and Chromium – 0.95) Other metals - BLQ(LOQ:0.002)	BDL (DL:2)	BDL (DL:4)	5.7	BDL (DL:2)

BDL – Below detection Limit *DL- Detection Limit*
BLQ-Below Limit of Quantification *LOQ-Limit of Quantification*

3.3. Aggregation and settling in static aqueous solutions

The settling of Al_2O_3NPs in aqueous solutions with varying pH are shown in Figure 5a. After 90mins of experimentation, the rate of settling of Al_2O_3NPs at pH 5 was greater than other pH conditions. The increase in the settling rate might be due to the suspension's pH being near to the point of zero charge (pHzpc) of Al_2O_3NPs (Figure 7a). The pHzpc of Al_2O_3NPs was found to be 5. As a result, at or near pHzpc, particles have little or no charge, resulting in a significant reduction of repulsive interactions between the Nanoparticles; hence, each contact between NPs and aggregates may promote particle adhesion which in turn results in the fast settling of particles (Chen and Elimelech 2006).

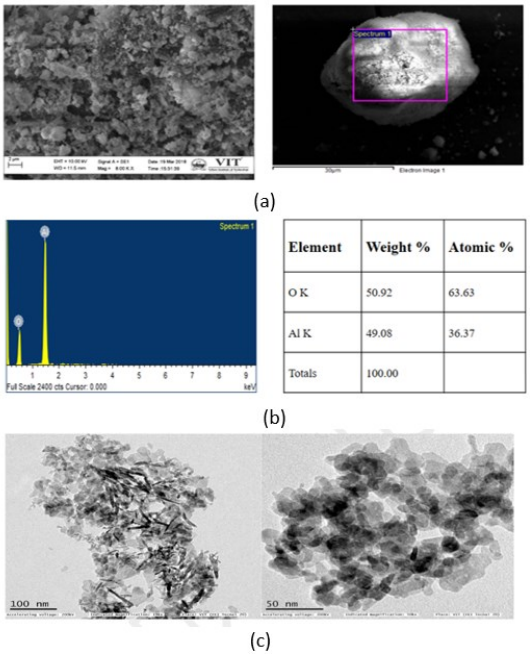

Figure 4. SEM (a) and EDX (b) analysis of Al_2O_3 (c)TEM image of Al_2O_3

The stability and aggregation of metallic nanoparticles in liquid solution are heavily influenced by type of the salt and IS. The influence of monovalent ions on the stability of Al_2O_3NPs was investigated using 10, 50 and 100 mM NaCl (Figure 5b) (Guzman *et al*. 2006; Zhang *et al*. 2008). The results show that the sedimentation of Al_2O_3NPs suspensions increased as the conc. of the electrolyte increased. Increasing the IS and monovalent ion concentration results in the compression of electrostatic double layer because of which the interparticle repulsion diminishes leading to greater aggregation and settling (Illés and Tombácz 2006; Zheng *et al*. 2019). Also, the increased IS altered the Vander Waals force of attraction between the particle as a result at higher IS the particle aggregate faster.

The sedimentation plots and the zeta potential are displayed (Figure 5c and Table 1). The zeta potential of the Al_2O_3NPs was changed with increasing HA conc. (Table 1) due to the carboxylic groups present in the HA(Tian et al. 2010). However, increased concentration of HA did not result in significant variation in settling in the analyzed time period. The result shows (Figure 5c) that stronger electrostatic and steric repulsive forces boosted the stability of the NPs as a result of the larger concentrations of negative charge on the Al_2O_3NPs surface. Thus, steric interactions and electrostatic repulsion all prevented nanoparticle agglomeration of Al_2O_3 in aqueous medium. The presence of HA increases the negative charges of Al_2O_3NPs, which results in stability rather than aggregation of the nanoparticles. According to the experimental results, there was less aggregation and sedimentation at the concentrations of 0.1 and 1 ppm than at 10 ppm HA (Vaˆnia Serra˜o Sousa 2013).

Figure 5d shows the sedimentation pattern of Al_2O_3NPs at varied particle concentration (10, 50 and 100ppm). The Al_2O_3NPs agglomerate fast at lower particle concentration of 10ppm. The results suggest that the change in the

particle concentration results in alteration of Al_2O_3 NPs sedimentation pattern (Khan *et al*. 2018). The zeta potential of particle for 100ppm was -28.07. Due to the presence of greater electrostatic force of repulsion the degree of colloidal stability of Al_2O_3 NPs was higher (Table1)

As shown in Figure 5e, the rate of sedimentation was higher in lake water compared to other natural water. The lake water that had been gathered was having a different chemical makeup when compared to all other natural waters as shown in (Table 3). The organic components, heavy metals, nutrients, and other elements present in the water might be absorbed and complexed by the nanoparticles, resulting in aggregates. The Al_2O_3NPs tend to settle out quickly because of the water's higher hardness. By changing the electrostatic repulsion and energy barriers, the lake water's 900 mg/L of chloride and 894 mg/L of calcium also may speed up the NPs' settling (Lanphere *et al*. 2014; Nanja *et al*. 2020; Zheng *et al*. 2019). Higher hardness and ionic concentrations in natural waters resulted in higher settling rates.

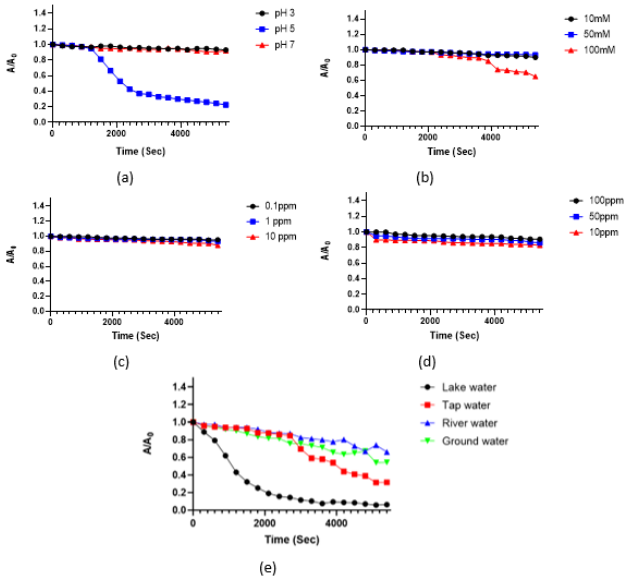

Figure 5. The sedimentation of Al_2O_3 NPs with varying parameters pH (3, 5 and 7) (5a), IS (10mM, 50mM and 100mM) (5b), HA (0.1mM, 1mM and 10mM) (5c), Particle Con. (10ppm, 50ppm and 100ppm) (5d) and natural water system (5e).

3.4. Effect of the environmental parameters on column transport

The influence of NPs concentration on the transport and retention in sand column was investigated for 3 distinct concentrations of NPs (10, 50 and 100ppm). While the inlet particle concentration rose from 10 to 100ppm, outlet particle concentration was also increased. At 4 PV, $C/C_0$was around 0.0803 for 100ppm and 0.0437 for 10 ppm, respectively. The breakthrough reached 0.0748 at 50ppm, but only after 6 PV (Figure 6a), As the concentration of NPs increase, a greater number of NPs will elute out of the column because the maximum solid retention capacity of the column is limited and greater number of the NPs stay unattached. As a result, more nanoparticles are eluted from the sand column at early pore capacities, resulting in higher nanoparticle concentration in the outlet (Davoudi *et al*. 2014; Phenrat *et al*. 2009; Rahman *et al*. 2013). Figure 6a clearly shows that as the concentration of NPs increase relatively more NPs are eluted out of the column.

Al_2O_3 NPs have greater retention at pH 3than at pH 7. The presence of hydrogen ions and the positive surface charge on the nanoparticles are the contributing factors for the greater retention of the NPs in the column because of the attraction to the negatively charged quartz sand (-32.2 mV). At pH5, which was determined to be the point of zero charge of the NPs, the retention is less when compared to pH3 and pH 7. The breakthrough C/C_0 of 0.097reached at 4 PV for pH 5 and 0.0505 at 4 PV for pH3. For pH 7 breakthrough was around 0.080345 at 4 PV (Zareei *et al*. 2019a) (Figure 6b).

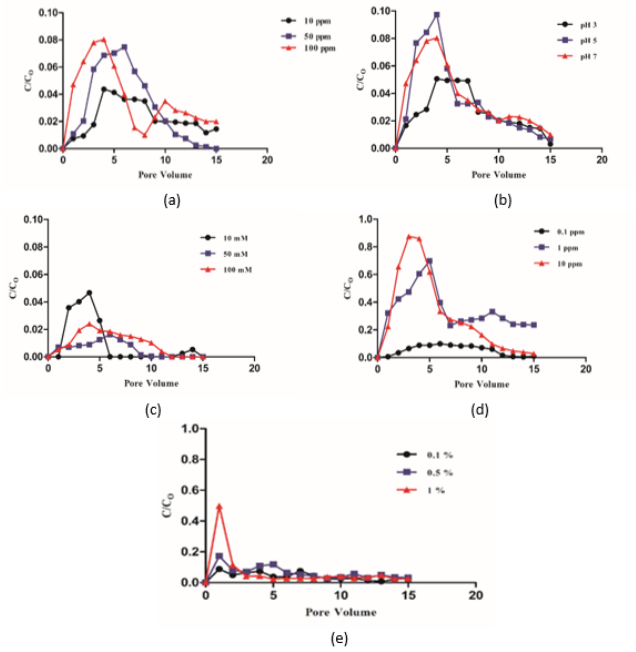

Figure 6. (a) Breakthrough curves for Al_2O_3 nanoparticles at varying particle concentration (10, 50, and 100ppm) in a background solution at 1000 µL/min flow rate.C_0 and C denotes concentrations of inlet and outlet nanoparticles, respectively. (b) Breakthrough curves for Al_2O_3 nanoparticles at varying pH of 3, 5 and 7in a background solution at 1000 µL/min flow rate.C_0 and C denotes concentrations of inlet and outlet nanoparticles, respectively. (c) Breakthrough curves of Al_2O_3 at different IS of 10 mM, 50 mM and 100mM in background solution at 1000 µL/min flow rate.C_0 and C represent nanoparticle concentrations in inlet and outlet, respectively. (d) Breakthrough curves for Al_2O_3Np for different Humic acid concentrations (0.1, 1, and 10 ppm) in background solution at 1000 µL/min flow rate.C_0 and C represent nanoparticle concentrations in inlet and outlet, respectively. (e) Breakthrough curves for Al_2O_3NPs for different concentrations of kaolinite (0.1, 0.5 and 1%) in background solution at 1000 µL/min flow rate.C_0 and C represent nanoparticle concentrations in inlet and outlet, respectively

The effect of monovalent and divalent cations and anions on the nanoparticle transport have been analyzed extensively for several nanoparticles. In this study, the effect of varying sodium chloride concentration has been evaluated. The change in ionic strength of the solution resulted in a significant variation in the zeta potential

values of the NPs with the10 ppm NaCl solution having the least positive zeta potential value which confers the least electrostatic attraction to the negatively charged sand particles when compared to highly positive charged solutions at 50 ppm and 100 ppm NaCl solution. Nanoparticle elution happened at a maximum C/C_0 of 0.0466 for 10 mM NaCl, followed by 100 mM at a maximum C/C_0 of 0.0254 and 50 mM NaCl at a maximum C/C_0 of 0.0162 with PV of 4, 6 and 4 respectively. Greater the ionic strength resulted in a considerable rise in particle retention, indicating that more nanoparticle attachments occur on the sand surface as the energy barrier decreases (Jones and Su 2014; Rahman *et al*. 2013; Zareei *et al*. 2019a).

In the presence of Humic acid, Al_2O_3 NPs gain a negative charge because of the absorption of HA onto the NPs. Due to electrostatic stabilization between the NPs and the negatively charged collector, Al_2O_3 mobility increased significantly in the presence of HA. Enhanced transport was demonstrated by C/C_0ratios approaching 0.099 with 6PV at 0.1ppm of humic acid, 0.875 with 3PV at 10ppm, and 0.697 with 5PV at 1ppm. In the presence of HA, the BTCs demonstrate a delayed breakthrough of Al_2O_3NPs (Figure 6c). The NOM yields a negative surface charge and electro-steric stability to the Al_2O_3 NPs due to the binding of carboxylic (COOH) and phenolic functional groups (R-OH) to the surface of particle, which enhanced the Al_2O_3 transit along column (Davoudi *et al*. 2014; He *et al*. 2020; Rahman *et al*. 2014). Also, the presence of HA increased the stability of the suspension and inhibits aggregation via improving electrostatic repulsion and steric hindrance as shown in the sedimentation experiments (Figure 6d).

Figure 6e depicts the profiles of Al_2O_3 breakthrough curves for the transport of Al_2O_3 NPs in kaolinite added porous media. Based on the data acquired, the presence of clay in the sand bed increased the retention of the NPs, which is in accordance with the transport profiles observed for other colloids in presence of natural clays. The increased retention is attributed to the surface charge heterogeneity of the kaolinite and the adsorption of the NPs to the clays (Bayat *et al*. 2015; Lu *et al*. 2017). However, the effect of variation of the solution chemistry on the clay charged porous media has to be evaluated further.

3.5. Effect of Natural water on the column transport

From the Figure 7, it can be seen that the content of Al_2O_3NPs in the effluent greatly decreases in both ground and tap water. For tap water, the effluent content (C/C_0) dropped from 0.027 to 0.0. Additionally, Al_2O_3 retention is almost 100% in the presence of groundwater. However, in the presence of lake and river water there was an increase in the Al_2O_3 effluent concentration. The electrostatic repulsion between the colloidal particles and the sand sediment decreased as the surface charge of nanoparticles turned positive in tap water. However, the retention was high in ground water even when a relatively high negative surface charge on the NPs was observed. Also, significantly higher aggregate size of NPs was observed in ground water which could be the contributing factor for higher retention (Khan *et al*. 2018; Nanja *et al*. 2020). The incidence of various ions in groundwater might also have a major impact on the transport behavior of NPs (Lanphere *et al*. 2014; Zheng *et al*. 2019). Although the hardness and the presence of chloride ion in the Lake water is high, increased transport of the NPs was observed. This is in contrast to the sedimentation experiments where the aggregation of NPs increased in presence of Lake water.

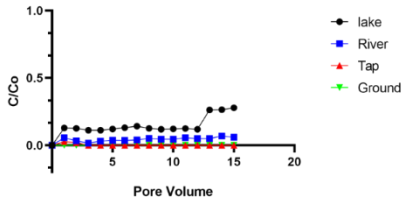

Figure 7. Breakthrough curves for Al_2O_3 nanoparticles with different natural water as background solution at 1000 µL/min flow rate.C_0 and C represent nanoparticle concentrations in inlet and outlet, respectively.

3.6. Mathematical model

3.6.1. DLVO theory

The DLVO curve represents the role of van der Waals and electrostatic interactions in the colloidal solution between particle-particle and particle to collector. A maximum interaction energy represents a strong barrier to aggregation and retention of the particle and indicates that colloidal charged particles are stable. However, the change in the surface charge of the nanoparticles, as well as the surface of the quartz sand, at different environmental parameters exert an influence on the interaction energies. In this study, at various pH, ionic strengths and HA concentrations, Al_2O_3 NPs and sand zeta potential was examined and tabulated (Table 1). In terms of dimensionless total interaction energy, the nanofluid with 100 ppm aluminium has the maximum on the DLVO curve than the other two concentrations (10 and 50ppm) indicating that the nanofluid is more stable at higher nanoparticle concentration.

Positive interaction energy levels in DLVO interaction profiles imply a repulsive situation, and energy values with negative interaction represent attraction. Positive energy barriers were seen at various Al_2O_3 NP concentrations, per DLVO calculations (10, 50 and 100ppm). Higher Φ max caused the particles to repel one another, which improved stability. In comparison to 10 and 50 ppm, stability was higher at 100 ppm particle concentration because the maximum was better (Figure 8a). As shown in Figure 8b, when Al_2O_3 NP was suspended in solution containing NaCl with concentrations of 10, 50, and 100 mM, positive interaction energy profiles were seen. The higher interaction energy values confirm that the colloidal stability is higher at 100mM NaCl circumstances (Table 4). The findings showed that the interactions between the Al_2O_3 NPs grew more repulsive at higher ionic strengths, resulting in higher stability (D. Ghosh *et al*. 2022). The overall interaction energy of Al_2O_3 NP at pH 3,5 and 7 were positive, as illustrated in Figure 8c. Primary minima revealed that when the energy barrier rose, the electrostatic repulsive forces increased, and relatively high

stability was seed in the aqueous matrix at pH 7. At pH 3 and 5, although the whole interaction energy was repulsive, relative to pH 7 the stability reduces. (Table 4)

Significant electrostatic repulsion was seen between Al_2O_3 NP when they were suspended in a solution containing HA at three different concentrations (0.1, 1 and 10 ppm) (Figure 8d). In presence of HA, positive interaction energy profiles were achieved and an increase in the height of energy barrier was seen with decreasing HA concentration. (Table 4). Greater Φ max was seen at 0.1 ppm of HA (4.165e-18 J). The enhanced electrostatic repulsion among the NPs induced by the higher energy barrier at 0.1ppm of HA prevented their aggregation and sedimentation. The DLVO interaction energy profiles showed that the addition of HA altered the stability and dispersity of Al_2O_3 NP, which is consistent with the high rate of settling at higher HA concentration (Figure 8c). Positive interaction energy profiles were noticed when Al_2O_3 NP were suspended in groundwater (Figure 8e). For river, lake and tap water, the van der Waals interaction dominate and the energy barrier is minimum (Table 4). The Al_2O_3 NPs suspended in ground water took relatively longer time intervals to settle when compared to lake water where the aggregation and sedimentation rate was higher.

Table 4. DLVO interaction energy profiles for Al_2O_3 NP–NP and NP- quartz sand particle interaction as a function of separation distance at different background solution

Background solution	Size (µm) p_r	Maximum energy barrier Φ max (J) of Al_2O_3 NP–NP interaction	Maximum energy barrier Φ max (J) Al_2O_3 NP–quartz sand particle interaction
pH3	0.108	7.2444e-19	4.551e-19
pH5	0.204	1.2538e-18	7.614e-19
pH7	0.304	12.1478e-18	1.317e-18
10 ppm	0.227	1.5896e-18	1.0135e-18
50 ppm	0.182	1.3462e-18	8.7189e-19
100 ppm	0.4955	3.855e-18	2.5346e-18
10mM NaCl	0.336	7.7165e-19	2.667e-19
50mM NaCl	0.583	4.0246e-18	2.5545e-18
100mM NaCl	0.722	5.4318e-18	3.5336e-18
0.1 ppm HA	0.530	4.165e-18	2.7421e-18
1 ppm HA	0.305	2.1757e-18	1.3949e-18
10 ppm HA	0.220	2.2431e-18	1.5468e-18
Ground	8.2	3.9799e-17	3.9799e-18
Lake	4.25	0	0
River	1.061	9.9011e-19	1.4668e-19
Tap	2.09	0	0

The energy barrier for the NP-quartz interaction was reported for 10, 50, and 100 mM NaCl in Figure 9a and 9b. According to these calculations, the energy barrier (Table 4) for aluminium oxide nanoparticles approaching a sand surface increases as the ionic strength rises, resulting in a higher repulsion at an ionic strength of 100 mM than 50 mM and 10mM (Lin and Wiesner 2012). The computed interaction energy profiles agree with the lesser deposition pattern (10 mM >50 mM >100 mM) (S. Ghosh *et al*. 2008; Mikelonis *et al*. 2016).

According to Figure 9c the NP's exhibits positive interaction energy with lesser energy barrier (Table 4) on the DLVO curve with variation in pH values. Although, at all the pH values evaluated the retention is higher, the highest retention was observed at pH 3 which correlates well with the Breakthrough profile for varying pH in Figure 6b (Zareei *et al*. 2019b).

In the nanofluid, the total interaction energy between Al_2O_3 and quartz sand in presence of HA reduces indicating the increasing stability and elution of the nanoparticles. According to the computed interaction energies, 0.1ppm HA has a maximum interaction energy than 1 ppm and 10 ppm HA (Figure 9d). These values deviate from the breakthrough curve values for Humic acid (Figure 6d) which indicate higher retention with 0.1 ppm HA.

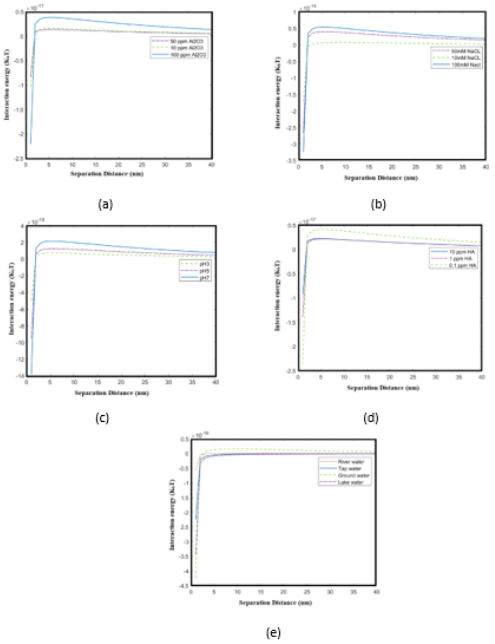

Figure 8. Interaction profiles yielded with DLVO theory for Al2O3 NP–NP interaction as a function of separation distance. (a) at different particle concentration (10,50,100 ppm Al2O3). (b) At different NaCl (10, 50, 100 mM). (c) At different pH condition (3, 5, 7 pH). (d) At different HA concentration (0.1, 1, 10 ppm). (e) Different natural water

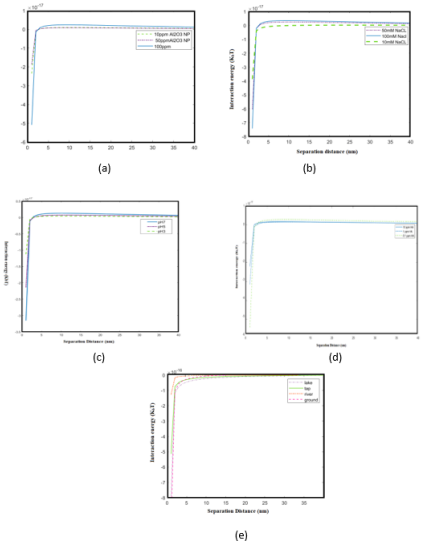

Figure 9. Interaction profiles yielded with DLVO theory for Al_2O_3NP–quartz sand particle interaction as a function of separation distance. (a) at different particle concentration (10,50,100 ppm Al_2O_3). (b) At different NaCl (10, 50, 100 mM). (c) At different pH condition (3, 5, 7 pH). (d) At different HA concentration (0.1, 1, 10 ppm)

Positive interaction energy profiles were seen when Al_2O_3 NPs were suspended in groundwater, river, lake, and tap water, however they had extremely low energy barriers. It was anticipated that the van der Waals force of attraction would greatly rise given the high deposition rate (Table 4). Al_2O_3 NPs became more attracted to one another as a result, which led to longer-term aggregation and retention in the case of tap, ground, and river water (Figure 9e). It is evident that the Al_2O3 NPs'- sand interaction energy barrier made it easier for them to deposit in the presence of natural water. All water except ground water experiences virtually the same rate of Al_2O_3 NPs aggregation. Due to the hardness of the water, which causes steric repulsion and electrostatic repulsion, the rate of aggregation and deposition for ground water varies from other natural waters (Figure 9e) (Degenkolb *et al*. 2019; Nanja *et al*. 2020).

3.6.2. Evaluation of particle retention in porous media by CFT

Colloidal transport across porous media is heavily dependent on the deposition and entrapment of the particles in the porous media. A thorough understanding of deposition of colloidal particle is required for predicting their transit in natural porous media. As per CFT, the deposition rate can be estimated from the attachment efficiency(α) and single collector efficiency(η0). α can be computed during the adsorption procedure at varying electrostatic conditions by using the C/C_0rateattainedat breakthrough from the investigational BTCs. The following constants were used in these calculations: Collector diameter (d_c)- 0.300mm, fluid approach velocity (U)-1.0E-04, density of the nanoparticle(ρ_p)- 3880 kg/m3, fluid density (ρ_f) - 1000 kg/m3, fluid viscosity (μ) – 1.005E-3 kg/m3, Temperature (*T*) – 293 K, porosity(*f*) – 0.36, Hamaker constant (*A*) – 6.8E-20J and Happel model parameter (*As*)- 49.10. Table 5 shows the parameters computed via CFT. Table 5 also includes d_p (dispersed particle average size solution) and C/C_0 values for a better understanding of particle movement in porous media (Zareei *et al*. 2019a).

Table 5. Parameters used for CFT and the retention coefficients measured from BCTs under various experimental conditions

Parameters	Particle size (μm)	C/C_0	η_I	η_G	η_D	Collector efficiency η_0	Attachment efficiency α	Deposition rate k_d
pH 3	0.216	0.01	1.2E-04	4.2E-04	1.7E-02	1.713E-02	1.680	2.56E-02
pH 5	0.408	0.03	2.9E-04	1.5E-03	1.0E-02	1.177E-02	1.861	1.95E-02
pH 7	0.608	0.042	5.1E-04	3.3E-03	7.3E-03	1.106E-02	1.791	1.76E-02
10 mM	0.672	0.035	5.8E-04	4.0E-03	6.7E-03	1.130E-02	1.854	1.86E-02
50 mM	1.166	0.007	1.3E-03	1.2E-02	4.3E-03	1.751E-02	1.771	2.76E-02
100 mM	1.444	0.01	1.7E-03	1.8E-02	3.7E-03	2.355E-02	1.222	2.56E-02
0.1 ppm HA	1.06	0.1	1.1E-03	9.8E-03	4.7E-03	1.564E-02	0.920	1.28E-02
1 ppm HA	0.61	0.3	5.1E-04	3.3E-03	7.3E-03	1.107E-02	0.680	6.69E-03
10 ppm HA	0.441	0.22	3.2E-04	1.7E-03	9.4E-03	1.146E-02	0.826	8.41E-03
10 ppm	0.454	0.013	3.3E-04	1.8E-03	9.2E-03	1.136E-02	2.390	2.41E-02
50 ppm	0.365	0.01	2.4E-04	1.2E-03	1.1E-02	1.237E-02	2.328	2.56E-02
100 ppm	0.991	0.045	1.0E-03	8.6E-03	4.9E-03	1.457E-02	1.330	1.72E-02
Ground water	16.45	0.076	5.6E-02	2.2E+00	5.3E-04	2.301E+00	0.007	1.43E-02
Lake water	8.512	0.12	2.2E-02	6.1E-01	8.9E-04	6.316E-01	0.021	1.18E-02
River water	2.123	0.05	3.0E-03	3.9E-02	2.7E-03	4.462E-02	0.420	1.66E-02
Tap water	4.191	0.02	7.9E-03	1.5E-01	1.6E-03	1.592E-01	0.154	2.17E-02

Although several mechanisms contribute to the retention of the nanoparticles, three key processes: interception, sedimentation and diffusion contribute significantly (Ostrovsky *et al*. 2014). Filtration theory estimates the contribution of these mechanisms represented by ηI for interception, ηG for sedimentation and ηD for diffusion. (Table 5). With increase in particles size, generally resulted in decline of interception efficiency (η_I) and gravity efficiency (η_G) but dispersion efficiency increased. The attachment efficiencies for 10 ppm and 50 ppm nanoparticle concentrations are higher and significantly different from 100 ppm nanoparticle concentration which

is in correlation with the retention profiles (BTCs) observed where the 100 ppm nanoparticles concentration showed increased transport of the nanoparticles. For varying pH, pH3 showed an increase in collector efficiency which translated into higher deposition rate although the attachment efficiency is not showing high variation when compared to other pH values evaluated.

As shown in Table 5, particle transit in a background solution containing 50mM NaCl resulted in the highest retention and the least deposition rate was observed at 10 mM. With varying humic acid concentrations, addition of 0.1 mg/L HA acid increased the transport of the nanoparticles compared to neutral conditions but as the HA concentration was increased to 10 ppm the retention of the nanoparticles increased. The presence of HA facilitated the transport of the nanoparticles when compared to all other environmental parameters analyzed here which is consistent with the results cited by several reports (Grolimund *et al*. 1998; Rahman *et al*. 2013).

For natural waters, tap water showed the highest deposition rate which is consistent with the breakthrough profiles however, the deposition rate for ground water showed a lower value although the collector efficiency showed very high value representing that although the attachment efficiency i.e. the effect of surface charge on the retention process is low, higher retention were observed because of the increase in collector efficiency which indicates that the larger size of the alumina nanoparticles in the ground water led to higher retention although conditions for attachment are not favorable.

4. Conclusion

The aggregation rates and transport of Al2O3 nanoparticles in aqueous media and experimental column investigations emphasized that varying the pH, IS, HA and amount of nanoparticle will alter the transport of the Al2O3nanoparticles. Although, the effect of these parameters on transport in porous media are well established, the effect of these on the static aqueous conditions are not available for Al2O3 which gap is bridged by this study. Physical tests have shown that under the solution chemistries studied, the Al2O3 are mostly stable in aqueous media but the stability drastically varies in presence of natural waters. In case of transport of Al2O3, in the natural water system the particleretention is higher. These results show that a under natural water systems, the NPs tend to aggregate and settle in aqueous media and are retained in the porous media. However, a thorough understanding of the natural water systems are further required to evaluate and predict the behavior of the NPs in complex natural environments

Statements and Declarations

Acknowledgment

The authors would like to thank Centre for Nanobiotechnology (CNBT), and Vellore Institute of Technology for extending their support to this study.

Conflicts of interest

The authors declare no conflicts of interest.

Data policy

All data generated or analyzed during this study are included in this published article.

Funding information

The author declare that this study had financial support for research, provided by the Department of Science and Technology-Science and Engineering Research Board (DST-SERB) grant number YSS/2015/000179**.**

Abbreviation

η_0	Single collector efficiency
d_c	The average size of collector particles
K_{att}	Particle deposition rate coefficient
ADE	Advection-dispersion equation
BDL	Below detection Limit
BLQ	Below Limit of Quantification
C, S	Concentrations of the nanoparticles in the liquid and solid phase respectively
C_0 and C_L	particle concentrations in the inlet and outlet
CFT	Clean bed filtration model
D	Coefficient of Hydrodynamic dispersion
DI	Distilled water
DL	Detection Limit
DLVO	Derjaguin–Landau–Verwey–Overbeek
EDX	Energy Dispersive X-Ray Analysis
ENP's	Engineered nanoparticles
FTIR	Fourier Transform Infrared spectroscopy
HA	Humic Acid
IS	Ionic strength
k_d	Deposition rate
L	column height
LOQ	Limit of Quantification
mg/L	milligram per litter
nm	Nano meter
NOM	Natural organic matter
Np's	Nanoparticles
SEM	Scanning Electron Microscope
TEM	Transmission Electron Microscope
XRD	X-ray diffraction
v	Particle velocity
α	Attachment efficiency
ε-	porosity
θ_W	porosity of the column
ρb	Bulk density of porous medium

References

Alamouti A. F., Nadafan M., Dehghani Z., Ara M. H. M. and Noghreiyan A. V. (2021). Structural and Optical Coefficients Investigation of γ-Al2O3 Nanoparticles using Kramers-Kronig Relations and Z–scan Technique, *Journal of Asian ceramic societies*, **9(1)**: 366–373.

Bayat A. E., Junin R., Mohsin R., Hokmabadi M. and Shamshirband S. (2015). Influence of clay particles on Al_2O_3 and TiO_2 nanoparticles transport and retention through limestone porous media: measurements and mechanisms, *Journal of Nanoparticle Research,* **17(5)**: 1–14**.**

Chen K. L. and Elimelech M.(2006). Aggregation and Deposition Kinetics of Fullerene (C60) Nanoparticles. *Langmuir,* **22(26)**: 10994–11001.

Davoudi A., Salehpour A. and Habibi A. (2014). Transport and Deposition of Alumina Nanoparticles in Water Saturated

Porous Media: An Experimental Study, *Journal of Dispersion Science and Technology,* **35(9)**: 1339–1344.

Degenkolb L., Dippon U., Pabst S. and Klitzke S. (2019). Transport and retention of differently coated CeO 2 nanoparticles in saturated sediment columns under laboratory and near-natural conditions, 15905–15919.

Derjaguin B. V. and L. Landau. (1941). Theory of stability of strongly charged lyophobic sols and of the adhesion of strongly charged particles in solutions of electrolytes. *Acta Physico-Chimica Sinica*, **17**:633–662.

Ghosh D., Das S., Kumar V., Pulimi M., Anand S., Chandrasekaran N., et al. (2022). Nano-SiO 2 transport and retention in saturated porous medium : Influence of pH, ionic strength, and natural organics, *Journal of contaminant hydrology*, **248**(May): 104029.

Ghosh S., Mashayekhi H., Pan B., Bhowmik P. and Xing B. (2008). Colloidal behavior of aluminum oxide nanoparticles as affected by pH and natural organic matter, *Langmuir*, **24(21)**: 12385–12391

Gregory J. (1981). Approximate expressions for retarded van der Waals interaction, *Journal of Colloid And Interface Science.,* **83(1)**: 138–145.

Grolimund D., Elimelech M., Borkovec M., Barmettler K., Kretzschmar R. and Sticher H. (1998). Transport of in situ mobilized colloidal particles in packed soil columns. *Environmental Science & Technology,* **32(22)**: 3562–3569 .

Guzman K. A. D., Finnegan M. P. and Banfield J. F.(2006). Influence of surface potential on aggregation and transport of titania nanoparticles, *Environmental Science & Technology*, **40(24)**: 7688–7693.

Hassanpour P., Panahi Y., Ebrahimi-Kalan A., Akbarzadeh A., Davaran S., Nasibova A. N. et al. (2018). Biomedical applications of aluminium oxide nanoparticles. *Micro and Nano Letters*, **13(9)**: 1227–1231.

He J., Wang D., Fan T. and Zhou D. (2020). Cotransport of Cu with graphene oxide in saturated porous media with varying degrees of geochemical heterogeneity. *Water (Switzerland),* **12(2)**: 1–10.

Hogg R., Healy T. W. and Fuerstenau D. W. (1966). Mutual coagulation of colloidal dispersions. *Transactions of the Faraday Society,* **62(615)**: 1638–1651.

Illés E. and Tombácz E. (2006). The effect of humic acid adsorption on pH-dependent surface charging and aggregation of magnetite nanoparticles, *Journal of Colloid And Interface Science,* **295(1)**: 115–123.

Jiang J., Oberdörster G. and Biswas P.(2009). Characterization of size, surface charge, and agglomeration state of nanoparticle dispersions for toxicological studies, *Journal of Nanoparticle Research,* **11(1)**:77–89

Jones E. H. and Su C. (2014). Transport and retention of zinc oxide nanoparticles in porous media: Effects of natural organic matter versus natural organic ligands at circumneutral pH. *Journal of hazardous materials,* **275**: 79–88

Kang J. K., Yi I. G., Park J. A., Kim S. B., Kim H., Han Y. et al. (2015). Transport of carboxyl-functionalized carbon black nanoparticles in saturated porous media: Column experiments and model analyses, *Journal of contaminant hydrology*, **177–178**: 194–205.

Khan R., Inam M. A., Zam S. Z., Park D. R. and Yeom I. T. (2018). Assessment of Key Environmental Factors Influencing the Sedimentation and Aggregation Behavior of Zinc Oxide Nanoparticles in Aquatic Environment, *Water*. 1–18**.**

Kumari D. and Rychoudhury T.(2020). sediment in the presence of humic acid and under the groundwater condition Transport behaviour of different metal-based nanoparticles through natural sediment in the presence of humic acid and under the groundwater condition, *Journal of Earth System Science*,**129**:145.

Kumari J., Chandrasekaran N., Nagarajan R. and Mukherjee A.(2016). Individual, co-transport and deposition of TiO2 and ZnO nanoparticles over quartz sand coated with consortium biofilm, *Journal of environmental chemical engineering*, **4(4)**:3954–3960.

Lanphere J. D., Rogers B., Luth C., Bolster C. H. and Walker S. L. (2014). *Environmental nanomaterials*, **31(5)**, 1–10**.**

Lin S. and Wiesner M. R. (2012). Deposition of aggregated nanoparticles - A theoretical and experimental study on the effect of aggregation state on the affinity between nanoparticles and a collector surface, *Environmental Science & Technology*, **46(24)**: 13270–13277.

Lu T., Gilfedder B., Peng H., Peiffer S., Papastavrou G., Ottermann K. and Frei S. (2021). Relevance of Iron Oxyhydroxide and Pore Water Chemistry on the Mobility of Nanoplastic Particles in Water-Saturated Porous Media Environments, *Water, Air and Soil Pollution*, 232.

Lu T., Xia T., Qi Y., Zhang C. and Chen W.(2017). Effects of clay minerals on transport of graphene oxide in saturated porous media, *Environmental Toxicology and Chemistry*, **36(3)**: 655–660.

Mikelonis A. M., Youn S. and Lawler D. F. (2016). DLVO Approximation Methods for Predicting the Attachment of Silver Nanoparticles to Ceramic Membranes, *Langmuir,* **32(7)**, 1723–1731.

Nanja A. F., Focke W. W. and Musee N. (2020). Aggregation and dissolution of aluminium oxide and copper oxide nanoparticles in natural aqueous matrixes, *SN Applied Sciences*, **2(7**): 1–16

Nila A. S. S. (2018). Synthesis and XRD, FTIR Studies of Alumina Nanoparticle using Co-precipitation Method, *International Journal for Research in Applied Science and Engineering Technology*, **6(3)**: 2493–2496.

Ostrovsky I. S., Oceanographic I., Yacobi Y. Z. and Oceanographic I. (2014), *Lake Kinneret: ecology and management* **6**.

Phenrat T., Kim H.-J., Fagerlund F., Illangasekare T., Tilton R. D. and Lowry G. V. (2009). Particle size distribution, concentration, and magnetic attraction affect transport of polymer-modified Fe(0) nanoparticles in sand columns. *Environmental Science & Technology*, **43(13)**: 5079–5085.

Prashanth P. A., Raveendra R. S., Hari Krishna R., Ananda S., Bhagya N. P., Nagabhushana B. M. et al. (2015). Synthesis, characterizations, antibacterial and photoluminescence studies of solution combustion-derived α-Al 2 O 3 nanoparticles, *Journal of Asian ceramic societies*, **3(3)**: 345–351.

Rahman T., George J., Shipley H. J.(2013). Transport of aluminum oxide nanoparticles in saturated sand: Effects of ionic strength, flow rate, and nanoparticle concentration, *Science of the Total Environment*, **463–464**: 565–571.

Rahman T., Millwater H., Shipley H. J. (2014). Modeling and sensitivity analysis on the transport of aluminum oxide nanoparticles in saturated sand: Effects of ionic strength, flow

rate, and nanoparticle concentration, *Science of the Total Environment*, **499(1)**: 402–412.

Solovitch N., Labille J., Rose J., Chaurand P., Borschneck D., Wiesner M. R., Bottero J. Y. (2010). Concurrent aggregation and deposition of TiO2 nanoparticles in a sandy porous media. *Environmental Science & Technology,* **44(13)**, 4897–4902

Sun P., Zhang K., Fang J., Lin D., Wang M., Han J. (2015). Transport of TiO2 nanoparticles in soil in the presence of surfactants. *Science of the Total Environment*, **527–528**: 420–428

Tian Y., Gao B., Silvera-Batista C., Ziegler K. J. (2010). Transport of engineered nanoparticles in saturated porous media. *Journal of Nanoparticle Research*, **12(7)**: 2371–2380**.**

Tufenkji N., Elimelech M. (2004). Deviation from the classical colloid filtration theory in the presence of repulsive DLVO interactions. *Langmuir*, **20(25)**: 10818–10828

Vaˆnia Serra˜o Sousa.(2013). Aggregation kinetics and surface charge of CuO, *Journal of Environmental Chemistry*, **10**, 313–322.

Verwey E. J., Overbeek J. T. G., Nes K. van. (1948). Theory of the stability of lyophobic colloids: the interaction of sol particles having an electric double layer.

Witharana S., Hodges C., Xu D., Lai X., Ding Y. (2012). Aggregation and settling in aqueous polydisperse alumina nanoparticle suspensions. *Journal of Nanoparticle Research*, **14(5)**, 1–19.

Zareei M., Yoozbashizadeh H., Madaah Hosseini H. R., (2019a). The effect of pH and ionic strength on the transport of alumina nanofluids in water-saturated porous media: Experimental and modeling study, *Journal of Thermal Analysis and Calorimetry,* **137(4)**: 1169–1179.

Zareei M., Yoozbashizadeh H., Madaah Hosseini H. R. (2019b). Investigating the effects of pH, surfactant and ionic strength on the stability of alumina/water nanofluids using DLVO theory, *Journal of Thermal Analysis and Calorimetry*, **135(2)**: 1185–1196.

Zhang Y., Chen Y., Westerhoff P., Hristovski K., Crittenden J. C.(2008). Stability of commercial metal oxide nanoparticles in water, *Water* research **42(8–9)**: 2204–2212.

Zheng X., Li Y., Chen D., Zheng A., Que Q. (2019). Study on analysis and sedimentation of alumina nanoparticles. *International Journal of* Environmental *Research and Public Health,* 16(3).

Zhou D., Keller A. A. (2010). Role of morphology in the aggregation kinetics of ZnO nanoparticles, *Water research*, **44(9)**: 2948–2956.